Sensing Humidity Using Nanostructured SiO Posts: Mechanism and Optimization

Andy T. Wu[1]* and Michael J. Brett

Department of Electrical and Computer Engineering, University of Alberta, Edmonton, AB, Canada, T6G 2G7
[1]Jefferson Lab, MS58, 12000 Jefferson Avenue, Newport News, VA23606, USA

Recently it was demonstrated that relative humidity (RH) could be sensed using SiO films fabricated by a newly developed glancing angle deposition (GLAD) technique that enables three-dimensional control of the film microstructure on a 10 nm scale. The performance of the SiO sensors depends critically on their detailed microstructures. A surprising dynamic response range over five orders of magnitude was detected for a SiO sensor with a microstructure of posts and a porosity of 25%. This paper presents a detailed model for the new SiO sensors and reports the optimization of their sensing characteristics. The model is based on a modification of Sillars' medium theory incorporating the effects of the net heat of adsorption of water molecules, changes in conductivity at the interface between SiO and water molecules, water condensation inside the pores due to the capillary effect, changes in conductivity of the condensed water with RH, and pore size distribution on the performance of the sensors in the model. The model predicts that the sensing characteristics of a porous RH sensor are determined mainly by the microstructure of the medium and the complicated properties at and near the interfaces between the medium and the adsorbed or condensed water molecules. Although the model is developed to explain the sensing characteristics of our sensors, it is quite general and can be used to predict and explain the sensing characteristics for any other capacitive humidity sensor with a porous medium as the sensing material. The results of optimized sensors based on the guidance provided by the theoretical model are presented.

---

*Corresponding author, e-mail address: andywu@jlab.org

1.   Introduction

Recently, a new film deposition technique called glancing angle deposition (GLAD) was developed[1] at the University of Alberta. This technique is able to produce films with three-dimensional control of film microstructure on the 10 nm scale and with porosity controllable from 10 to 80%. We have used relative humidity (RH) sensing as an example[2,3] to demonstrate the power of this GLAD technique in various sensing applications. The sensing characteristics of the capacitive SiO sensors fabricated by the GLAD technique were found[2,3] to depend critically on the details of the sensors' microstructures. A dynamic response range over five orders of magnitude was detected for a sensor with a microstructure of cylindrical rods and a porosity of 25%. The sensor did not degrade after immersion in water and exhibited a response time of less than 3 s for a stepwise change of RH from 15% to 80%. On the other hand, the sensor showed a large undesirable hysteresis loop. Optimization was not successful since the relationship between the sensing characteristics of the sensors and the details of their microstructures was not trivial and details of the sensing mechanism were unknown.

Conventionally the sensing characteristics of capacitive RH sensors are explained using the well-known equivalent circuit model. This model is, however, incapable of explaining certain cases[2-7] in which the interactions between the sensing material, water moisture, and the applied field become strong. Moreover, the crucial microstructure-related parameters such as, the diameter of the pores and the pore size distribution, normally do not show up in the formulation of the conventional equivalent circuit model. To remedy this, Shimizu *et al.*[5] introduced a computation program which demonstrated clearly the importance of the microstructure-related parameters in the formulation of a theoretical sensing model. A similar approach[6] was also adopted by Li *et al.* to explain the sensing characteristics of their porous $Sr_{1-x}La_xTiO_3$ sensors. However, these models still treated the system as a mixture of the independent condensed water and the sensing material, which might not be generally valid. The neglect of the effect of the adsorbed water molecules on the sensing characteristics of the sensors in the model was also not justified. Khanna and Nahar,[7] on the other hand, incorporated the interactions between the sensing material, water moisture, and the applied field using Sillars' medium theory[8] and successfully explained the sensing behavior of their porous Al_2O_3 sensors fabricated by anodization. This model did not, however, consider the effects of the pore size distribution and water condensation in the pores of the sensors on the sensing characteristics of their sensors, and the model was not applicable for RH values lower than the $(RH)_m$ at which water molecules form a complete monolayer on the surfaces of all pores. Furthermore, in Sillars' medium theory[8] it was assumed throughout the analysis that the dielectric constant of the system after mixing did not deviate significantly from its original value. It is therefore doubtful whether we can simply use Sillars' results without modifications. To the best of our knowledge, in all models reported in the literature the sensing materials are continuous with isolated pores within them, which is the opposite of the case presented herein. Normally the effects of variations of the net heat of adsorption of water molecules with RH and the changes in conductivity at the interface between the sensing materials and the adsorbed water molecules on the performance of sensors are also neglected. As shown

in this paper, these effects are very important and should be included in the formulation of any sensing model. In view of the present situation, we believe that there is a need to develop a new theoretical model for our sensors and for other capacitive sensors with porous sensing materials in general.

In this paper, we present the detailed process of the development of RH sensors employing the GLAD technique with emphasis on the results of the development of a new theoretical model for explaining the sensing characteristics of our sensors and the results of optimization guided by the theoretical model. This model is based upon a modification of Sillars' medium theory incorporating the influences of the net heat of adsorption of water molecules, the change in conductance on the surface of SiO film after water adsorption, water condensation in the pores of the sensors due to the capillary effect, changes in conductivity of the condensed water with RH, and the pore size distribution on the sensing characteristics of the sensors into the model. The model is applicable for the entire RH range from dry to saturation. From this model, it is shown that indeed the pore size distribution and porosity have critical effects on the sensing characteristics of the sensors. By tailoring the detailed microstructure of the sensor according to the guidelines provided by the theoretical model, we have successfully minimized the undesirable large hysteresis loop observed previously[2,3] and explained each major behaviour of our sensors.

2. Experimental

Films of SiO were deposited by vacuum evaporation using the GLAD experimental set-up illustrated schematically in Fig. 1. The ϕ (azimuthal angle) rotation and α tilt of the substrate were accurately controlled by a computer. Films with controllable microstructures on the 10 nm scale and porosity from 10 to 80% could be grown with preset rotation speeds and tilting angles of the substrate. Further details may be found elsewhere.[1,9]

Figure 2 shows the layout of our sensors. First, aluminum was thermally deposited on the patterned surface of an insulating substrate to form the bottom electrode. To ensure good adhesion between the substrate and aluminum, the substrate was cleaned using the standard Pirahna process followed by cleaning with acetone, isopropyl alcohol, and baking dry. In between each cleaning step, ultrasonic cleaning using deionized water was performed. All of the cleaning processes were carried out in a class 100 clean room environment. Porous SiO films of various microstructures were then deposited by e-beam evaporation using the GLAD technique. This process was followed by the deposition of short and dense layers (called capping layers) to enable the subsequent deposition of the top electrode. The capping layers were formed by an exponential decrease of the incident flux angle with time through the continuous variation[1] of the angle α. Pieces of SiO with typical dimensions ranging from 3 to 6 mm and purity of 99.9% were used as source materials. The base pressure of the deposition chamber was typically 4.7×10^{-4} Pa and the deposition rate was manually controlled between 20 and 40 Å/S. Energy-dispersive X-ray analysis indicated that the films obtained were mainly SiO. Finally a patterned Au film was sputter-deposited through a shadow mask on top of the dense capping layer, thereby
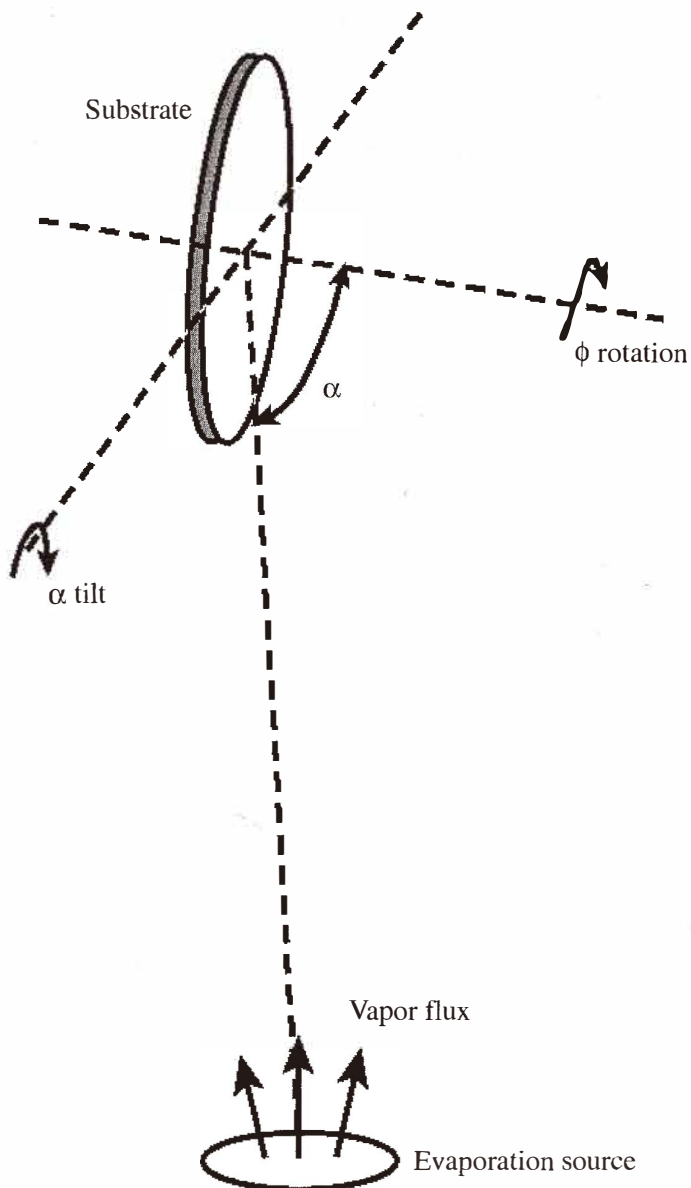
Fig. 1. Illustration of the GLAD apparatus.

forming the counterpart of the aluminum electrode as shown in Fig. 2. Capacitance-RH (C-RH) curves were measured at 120 Hz using the system described in ref. 3. Measurements were carried out at room temperature.
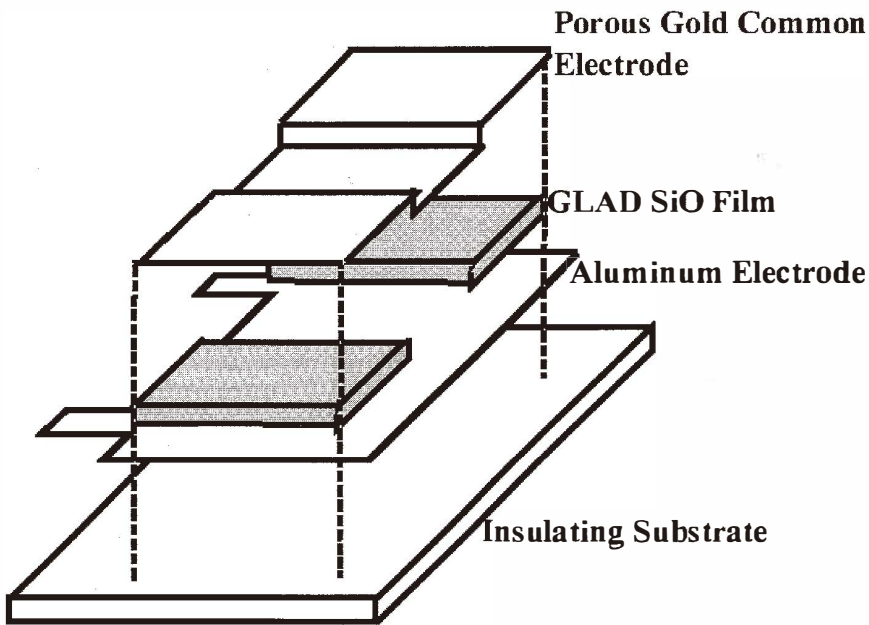
Fig. 2. Structure of our SiO RH sensor.

3.   Results and Discussion

In this section, we present details of the process of the development of RH sensors employing the GLAD technique. First we show the results of our study on the effects of microstructure on the sensing characteristics of the GLAD sensors, presenting some unique properties of our sensors which cannot be understood using the conventional equivalent circuit model. Then the theoretical model based on a modification of Sillars' medium theory is introduced. Issues associated with the effects of the microstructure of the sensor, the net heat of adsorption of water molecules on SiO walls, the applied field, and the conductivity near the interfaces between water molecules and SiO on the sensing characteristics, the stability of sensors, and the hysteresis of C-RH curves are discussed. General guidance for the optimization of the performance of porous RH sensors is given. Finally, the results of the sensors optimized and fabricated with guidance provided by the theoretical model are reported and compared with the calculated results.

3.1 *Effects of microstructure on sensing characteristics*
We first fabricated sensors with helical microstructures. A typical example of scanning electron microscope (SEM) cross-section images of sensors with helical microstructures is shown in Fig. 3(a). The helical SiO film was deposited obliquely at a tilt angle α of 83° utilizing substrate rotation to generate the helical turns. The corresponding C-RH curve is
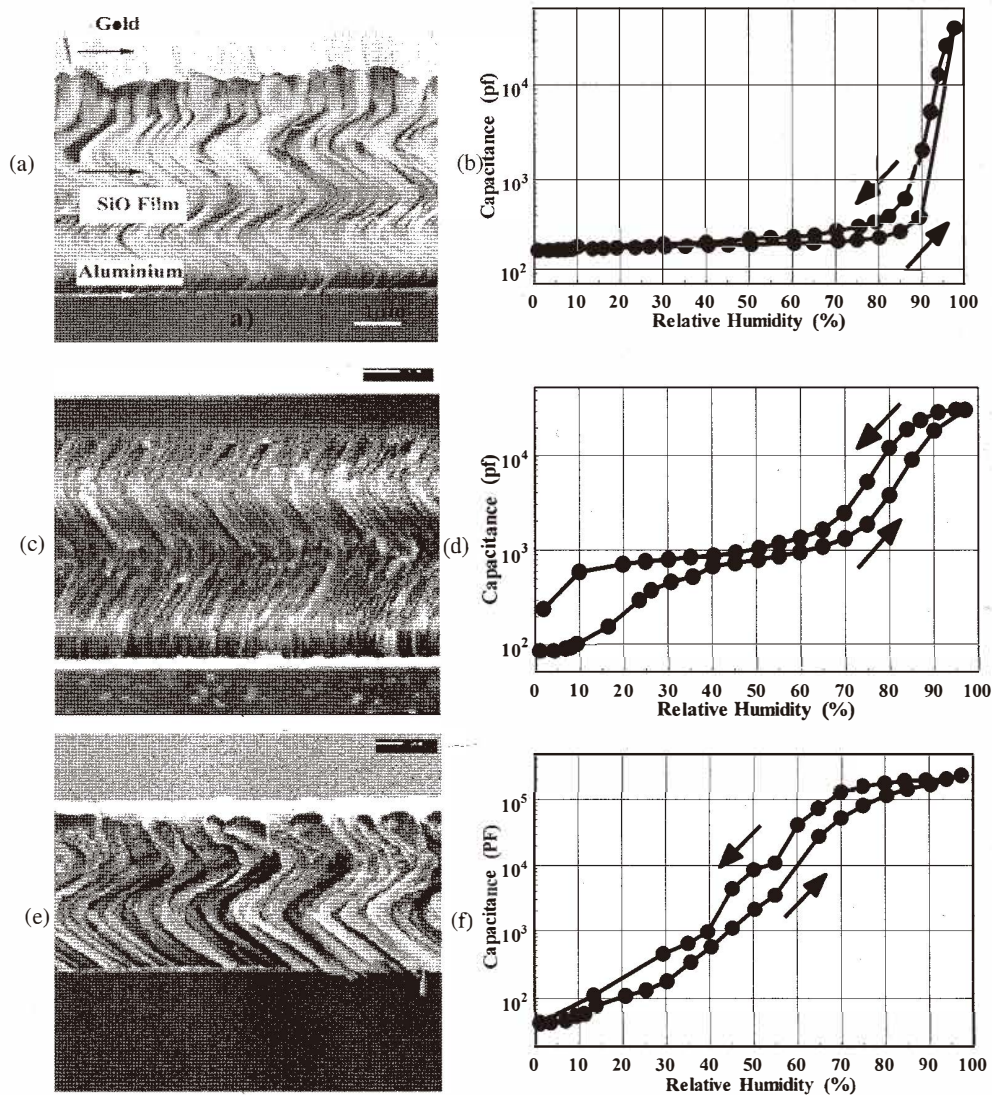
Fig. 3.   SEM cross-section images of a) sensor H1, c) sensor H2, and e) sensor H3 with the corresponding C-RH curves for b) sensor H1, d) sensor H2, and f) sensor H3.

shown in Fig. 3(b). Clearly, this sensor (sensor H1) shows low sensitivity between 1% and 85% RH. The capacitance has an undesirably large hysteresis loop between 50% and 97% RH. Below 85% RH, capacitance increases sharply, showing the nonlinear response of this sensor.

Our first target was to try to make the sensor response more linear. We considered that the increase in capacitance of the sensor was due to the increasing number of water molecules adsorbed or condensed inside the pores of the sensor, simply because the dielectric constant of the water molecule is much larger than that of SiO. Also from the work of Shimizu *et al.*,[5] we know that the sensing characteristics of the sensor can be adjusted by changing its microstructure. We therefore fabricated another sensor (sensor H2) at $\alpha = 81°$ with a similar helical microstructure. Figure 3(c) is the SEM cross-section image of sensor H2. Compared with Fig. 3(a), sensor H2 appears to be more compact than sensor H1, as expected, due to the smaller tilt angle $\alpha = 81°$. We therefore also expected that the corresponding C-RH curve would fall below the C-RH curve of sensor H1. This was, however, not the case as shown in Fig. 3(d). Although the C-RH curve did become slightly more linear than that of sensor H1, the hysteresis loop also became much broader. Moreover, the hysteresis loop did not recover fully after a cycle change of RH.

In further tests, we fabricated another sensor (sensor H3) at $\alpha = 85°$ to check the appearance of its C-RH curve. The SEM cross-section image of this sensor is shown in Fig. 3(e). Obviously, sensor H3 is the most porous sensor among the three shown here. As expected, this time the corresponding C-RH curve was located above that of sensor H1. However, the hysteresis loop covers the entire measured RH range and the dynamic response range is huge, covering four orders of magnitude. Thus it was observed that the relationship between the C-RH curve and the detailed microstructure of the GLAD sensor was not trivial, and a better understanding of the sensing mechanism was needed before an optimized sensor could be obtained.

Another issue that concerned us at the beginning of GLAD sensor development was the response time of the sensor. It is generally accepted that the quicker the response time, the better the sensor. The response time of an RH sensor is governed mainly by the diffusion time of the water molecules into the interior of the sensor, namely the interior of the GLAD SiO film. This implies that a sensor with a post microstructure should have a quicker response than a sensor with a helical microstructure. Acting on this idea, we fabricated a sensor (sensor P1) with a post microstructure at a deposition angle $\alpha = 85°$. Figure 4(a) is the SEM cross-section image of this sensor with the corresponding C-RH curve shown in Fig. 4(b). The measured response time for a step change in the RH from 15% to 80% is less than 3 s, which is the best among the sensors thus far described. Most surprisingly, the dynamic response range of sensor P1 covers over five orders of magnitude. To the best of our knowledge, this is the most sensitive RH sensor ever reported. It has been shown in refs. 2 and 3 that the conventional equivalent circuit model could not explain the unusually large change in capacitance.

Since the fabricated sensors here are new in terms of the sensing material, the fabrication technique, and the microstructures of the sensors, it is difficult to apply any existing sensing theories directly to this case without major modifications in order to explain the observed sensing characteristics. Development of a new sensing model may be required, particularly for explaining the observed wide dynamic response range of our sensors and for finding a way to minimize or eliminate the undesirably large hysteresis loops shown in Figs. 3 and 4. It was suggested in ref. 3 that any appropriate model should consider at least the following three effects on the sensing characteristics of the capacitive
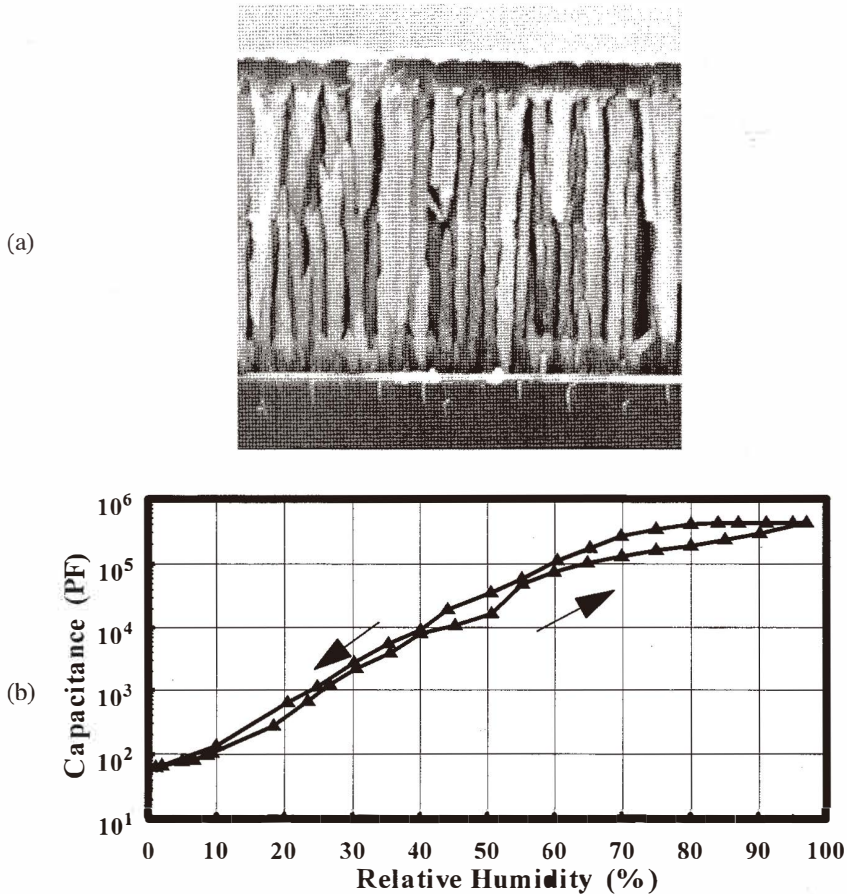
(a)

(b)

Fig. 4.   (a) SEM cross-section image of sensor P1 and (b) the corresponding C-RH curve.

SiO RH sensors: a) the effect of capillary condensation of water moisture inside the pores of the sensor, b) the effect of the detailed microstructure of the entire sensor, and c) the effect of the interactions between SiO film, water moisture, and the applied field.

3.2 *Theoretical model*

Among the three preconditions given for the sensing model, the last one is the most difficult to express mathematically. This problem is solved by Nahar *et al.*[4] and Khanna and Nahar[7] using the results of Sillars' medium theory.[8] Although we found that we need to modify the results of Sillars' medium theory in order to use them for explaining the sensing characteristics of our sensors, the work by Nahar *et al.*[4] and Khana and Nahar[7]

indicates a way to minimize mathematical calculations and expressions and is therefore a very important step towards the development of a complete theoretical model for RH sensing using porous media.

To start with, we assume that the sensor has a post microstructure similar to the one shown in Fig. 4(a). Clearly, water condensation inside the pores of the sensor plays an important role in terms of the sensing characteristics of the GLAD sensors. Mathematically, water condensation due to the capillary effect is described by the following well-known Kevin equation:

$$\ln \frac{P}{P_{\bullet}} = -\frac{2\gamma V \cos \phi}{r R_g T},$$

(1)

where P and $P_{\bullet}$ are the water vapor pressure and the vapor pressure at saturation, respectively. The term γ is the water surface tension, V the molar volume of the liquid water, r the radius of a cylindrical capillary, R_g the gas constant (8.31 J mole^{-1} K^{-1}), T the temperature, and ϕ the contact angle between liquid water and the walls of the capillary. This form of the Kevin equation is valid only for cylindrical capillaries or parallel-sided fissures.[10] For our case, we need to assume that the posts of our SiO GLAD films are in a close-packed situation in order to describe mathematically the water condensation inside the porous SiO films. This requirement leads to the first assumption of this model, which is that the microstructure of the sensor must be a packed structure of regular shapes such as, parallel close-packed posts, cubic packed spheres, orthorhombic packed spheres, rhombohedral packed spheres, tetragonal-spheroidal packed spheres, intersecting square capillaries or posts, or intersecting cylindrical capillaries or posts. For parallel close-packed posts, simple geometric consideration yields the following relationship between the radius of the posts (r_p) and r:

$$r_p = 7.30r.$$

(2)

In actual calculations, we have to first assume a certain post size distribution for the sensor, which may be estimated roughly from SEM cross-section images. The maximum number of layers of the adsorbed water molecules (n) can be determined using the following formula:

$$n = \frac{r}{2r_w},$$

(3)

where r_w is the radius of a water molecule. The total volume of water molecules (V) adsorbed on the surfaces of the pores inside the sensor is calculated using the following BET equation[11]

$$\frac{V}{V_{m}} = \left[\frac{c\left(P\big/P_{o}\right)}{1-\left(P\big/P_{o}\right)} \right] \left[\frac{1-(n+1)\left(P\big/P_{o}\right)^{n}+n\left(P\big/P_{o}\right)^{n+1}}{1+(c-1)\left(P\big/P_{o}\right)-c\left(P\big/P_{o}\right)^{n+1}} \right], \tag{4}$$

when RH is larger than $(RH)_m$. Here V_m is the total volume of water molecules inside the sensor when monolayer coverage is formed on the surfaces of all pores. The term c is defined as the following:

$$c = e^{\left(E_{1}-L\right)\big/R_{g}T}. \tag{5}$$

The terms E_1 and L are the heat of adsorption in the first layer and the latent heat of condensation, respectively. This means that c is essentially related to the net heat of adsorption. In our calculations, we use the following formula when $n \geq 10$.

$$\frac{V}{V_{m}} = \frac{c\left(P\big/P_{o}\right)}{\left[1-\left(P\big/P_{o}\right)\right]\left[1+(c-1)\left(P\big/P_{o}\right)\right]} \tag{6}$$

Once the post size distribution and the geometry of the sensor are fixed, Vm can be calculated simply by summation over contributions from posts of different radii where the surface area for each equivalent Kevin pore is $2\pi r d$. Here, d is the thickness of the porous film.

Now let us consider low RH. The sensing body may first be considered as a mixture of cylindrical SiO posts and air. Since the resultant dielectric constant ε_m does not change much from its value before mixing, the results of Sillars' medium theory[8] can be used. The value of ε_m may be expressed as:

$$\varepsilon_{m} = \varepsilon_{s}\left[1 + \frac{4\pi q_{a}\left(\varepsilon_{a}-\varepsilon_{s}\right)}{4\pi\varepsilon_{s}+\left(\varepsilon_{a}-\varepsilon_{s}\right)l_{a}} \right], \tag{7}$$

where ε_s and ε_a represent the dielectric constants of the compact SiO film and air, respectively. The term q_a is the percent of the total volume of air relative to the total volume of the sensor. The term l_a can be expressed[8] as

$$l_a = 4\pi \frac{r_a^2}{d^2}\left(\log\frac{2d}{r_a} - 1\right), \qquad (8)$$

when $d \gg r_a$. The value r_a is the radius of the cylindrical posts interspersed with air. At an arbitrary RH,

$$r_a = r - 2n_w r_w. \qquad (9)$$

Here n_w is the layer number of the adsorbed water molecules on the walls of the SiO posts. Under ideal dry conditions, $n_w = 0$.

If we put the sensor in a humid environment, water molecules enter the interior of the sensor. We know from our experimental results that the measured capacitance of the sensor increases enormously compared with its value before exposure to the humid environment. Therefore, we need to use a modified formula for the expression of the resultant dielectric constant of the sensing body ε. Simple derivation leads to the following formula for ε.

$$\varepsilon = \varepsilon_m \left\{ 1 + \frac{\left(4\pi q_w / l\right)\left\{(\varepsilon_w - \varepsilon_m)\left[\left(\frac{4\pi}{l} - 1\right)\varepsilon_m + \varepsilon_w\right] + \left(\frac{4\pi\sigma_w}{\omega}\right)^2\right\}}{\left[\left(\frac{4\pi}{l} - 1\right)\varepsilon_m + \varepsilon_w\right]^2 + \left(\frac{4\pi\sigma_w}{\omega}\right)^2} \right\} \qquad (10)$$

Here ε_w and σ_w are the dielectric constant and conductivity for pure water, respectively. The term q_w is the percent of the total volume of liquid water inside the sensor relative to the total volume of the sensor, and ω is the ac angular frequency. The value of l is defined as follows:

$$l = 2\pi \frac{r_{ew}^2}{d^2}\log(1/q_w), \qquad (11)$$

for film thickness $d \gg r_{ew}$. The term r_{ew} is the equivalent radius of the water cylindrical post and can be calculated using the following equation:

$$r_{ew} = \left\{\frac{4\pi r_w}{3\sqrt{3}}\sum_{i=1}^{n_w}\left[r - 2(i-1)r_w\right]\right\}^{\frac{1}{2}}. \qquad (12)$$

Here $r_{ew} \leq r$. For each post size, we can calculate the dielectric constant using Formula 10. The total dielectric constant of the sensor (ε_t) is simply the mathematical average over the contributions from different post sizes. Therefore, the total capacitance of the sensor (C_p) may be expressed as:

$$C_p = \varepsilon_t \varepsilon_o \frac{S}{2d},\tag{13}$$

where ε_o is the permittivity of free space and S is the area of the sensor.

During model calculations, we first need to determine the radius of the capillary, which allows water condensation to take place at a particular set RH using Formulae 1 and 2. Due to the uncertainty in Formula 1 at very low RH, we use it only for calculations above RH=30%. Therefore, for RH values smaller than 30% and larger than $(RH)_m$, we use Formulae 4 and 6 to determine the amount of water molecules adsorbed inside the pores of the sensor. For RH values larger than 30%, the total amount of water molecules is the sum of the amount of liquid water condensed due to the capillary effect and the amount of water molecules adsorbed on the walls of the posts for posts with radii larger than the largest radius that allows capillary water condensation to take place. Again, the latter contribution can be estimated using Formulae 4 and 6.

For values of RH lower than $(RH)_m$, the interactions between SiO films, water moisture, and the applied field are weak. References 2 and 3 have shown that under these conditions the conventional equivalent circuit model is valid. In refs. 2 and 3, the equivalent circuit model is considered only for dry and saturated cases. Here let us consider the sensor system at an arbitrary RH below $(RH)_m$. The equivalent circuit can now be drawn as in Fig. 5, where a detailed equivalent circuit is drawn only for the middle SiO posts. Simple circuit calculations show that C_p can be expressed as

$$C_p = \frac{C}{2\omega(R^2 + C^2)},\tag{14}$$

where ω is the angular frequency of the applied ac field. The terms R and C are defined as follows:

$$R = \frac{R_s + \omega^2 R_s^2 R_{wp} C_{ap}^2 + \omega^2 R_{wp}^2 R_s \left(C_{ap} + C_{wp}\right)^2}{B_{Rc}} + \mathrm{Re}\left(Z_t + Z_b\right)$$

$$C = \frac{\omega R_s^2 \left(C_s + C_{ap} + C_a\right) + \omega^3 R_{wp}^2 R_s^2 \left(C_{ap} + C_{wp}\right)\left[C_{ap}C_{wp} + \left(C_s + C_a\right)\left(C_{ap} + C_{wp}\right)\right]}{B_{RC}}$$
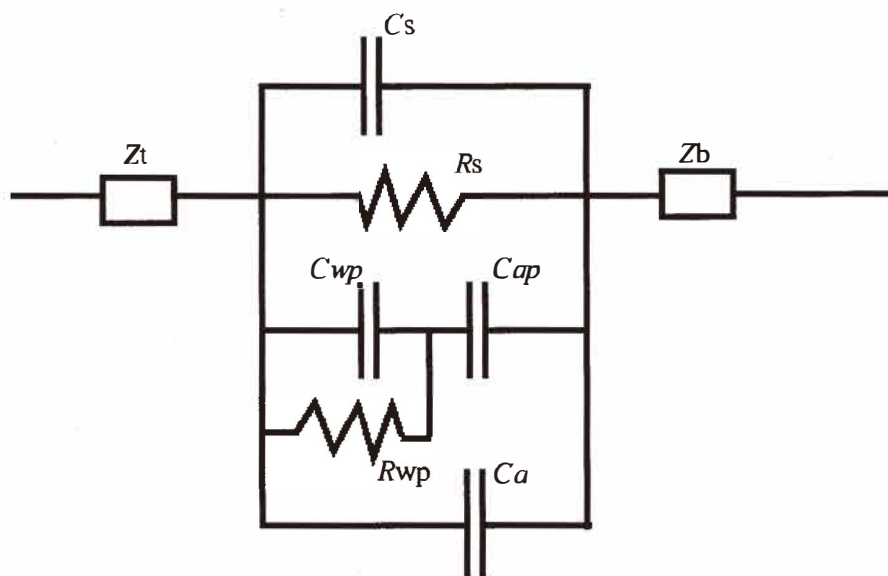$$- \mathrm{Im}(Z_t + Z_b)$$

Fig. 5.   Equivalent circuit of our SiO humidity sensor at an arbitrary RH below the RH at which water molecules form a monolayer on the porous surfaces of the sensor.

$$B_{RC} = \left\{1 - \omega^2 R_{wp} R_S \left[C_{wp} C_{ap} + (C_S + C_a)(C_{ap} + C_{wp})\right]\right\}^2$$
$$+ \omega^2 \left[(C_{ap} + C_a + C_S)R_S + (C_{ap} + C_{wp})R_{wp}\right]^2.$$

Here C_{wp} and R_{wp} are the contributions from the adsorbed water on the walls of the SiO posts with the corresponding contribution C_{ap} from air. C_a is the contribution of capacitance from the air for the remaining part of the pore space. The rest of the parameters are the same as those defined in ref. 3. It is easily seen that eq. 14 is the same as eq. 1 of ref. 3 under dry conditions. The amount of water molecules retained inside the pores of the sensor may be estimated by assuming a linear relationship between V and RH, since the interactions between water molecules are now weak.

It is noted that this equivalent circuit model may be used to determine accurately the average porosity of a porous medium by measuring its capacitance under dry conditions.

It is also important to point out again that the above treatments (except the equivalent circuit model) deal with the close-packed state only, under the condition that the sensing materials are not continuous as is the case for our GLAD sensors. Otherwise, the close-packed assumption is not required. In reality, however, the microstructures of the sensors are rarely in the close-packed state for sensors with isolated microstructures. We therefore

need to generalize the above treatments to include the nonclose-packed state. Take the post microstructure as an example. Suppose the porosity of the sensor is p, which can normally be measured using a porosimeter. The equivalent Kevin radius r_i for the ith post radius r_{pi} in the post size distribution function may now be obtained from the following eq. 10:

$$r_i = \frac{2pV_{ti}}{A_i},$$ (15)

where V_{ti} is the volume fraction of the sensor for a particular r_{pi}, which is known once the post size distribution function is assumed for the sensor. The term A_i is the corresponding surface area. Now we have to divide the discussion into two parts. When the porosity of the sensing material is larger than or equal to the close-packed porosity (p_c), the number of the posts (N_i) of a particular radius r_{pi} may be estimated from the following relationship:

$$N_i = \frac{(1-p)V_{ti}}{\pi r_{pi}^2 d}.$$ (16)

It is easy to show that r_i is related to r_{pi} in the following way:

$$r_i = f_i \frac{4}{3} \frac{p}{1-p} r_{pi}.$$ (17)

The term f_i is the ith correction factor for r_{pi} to ensure that, under close-packed conditions, eq. 2 holds. When $p < p_c$, we can always separate V_{ti} into two regions. One region is a compact film with zero porosity and the other is a close-packed film with porosity p_c. The volume of the latter region ($\gamma_{ci}=V_{ci}/V_{ti}$) may be estimated from the following relationship:

$$r_i = \frac{P}{P_c}.$$ (18)

The value of p_c can be obtained from the post size distribution function and the geometry of the sensor. For the close-packed portion of the film, eq. 2 is valid. The rest of the calculations are then the same as those in the case for the close-packed situation.

3.2.1 *An example of model calculations*

As an example, let us apply the above theoretical model to the case of sensor P1. For simplicity, it is assumed that there are only five post sizes with the distributions shown in

Table 1, and that the contact angle ϕ is zero. The first assumption is guided by the SEM cross-section image shown in Fig. 4(a), in which we can see that most of the posts have a size around 300 nm. We set the second peak in the distribution function to 25 nm to take the more compact bottom and top layers into account. It is common practice to assume the contact angle ϕ to be zero when using the Kevin equation, particularly in this case where ϕ is not available in the literature for SiO and liquid water. The value of p for this sensor[3] is about 25%.

For values of RH less than $(RH)_m$, the total capacitance can be calculated using Formula 14. First we need to know $(RH)_m$, which can generally be calculated using either Formula 4 or 6, depending on the post size. To do this, parameter c has to be known. Parameter c is related to the net heat of adsorption of water molecules on the walls of SiO posts through Formula 5. We could not find a measurement of the net heat of adsorption heat for water molecules on SiO in the literature. However, we may estimate it from the measured data in ref. 12 for SiO_2, which is found to be 2.8 kcal/mole. This leads to a value of 8.61% for $(RH)_m$.

For values of RH larger than $(RH)_m$, we use Formulae 4 and 6 to estimate the amount of water molecules adsorbed on the walls of pores when the pores are not filled with liquid water at a set RH. Formulae 1 and 2 are used to determine the pore size that can form liquid water at a set RH. In this particular case, the microstructure of the sensor is not in a close-packed situation. The Kevin radius should be determined using eq. 17.

A computational package based on the theoretical model presented above has been developed using software MatLab and Mathematica. The calculated C-RH curve for sensor P1 is shown in Fig. 6 together with the measured curve for comparison. The calculated curve correctly predicts the general tendency of the capacitance as a function of RH, in particular the large changes in capacitance. Strictly speaking, the calculated curve is for the adsorption branch of the measured curve only. We did not try to calculate the desorption branch of the C-RH curve, since it is much more complicated to do such calculations. This topic will be discussed later in this paper.

It is not unexpected to see that the calculated curve is above the experimental curve in Fig. 6. The major error comes from the calculation of the Kevin radius from the approximate relationship in eq. 17, which over-estimates the radius resulting in an over-estimation of the amount of water retained inside the sensor at a particular set RH. Other factors may include an over-simplified assumption of the pore size distribution function, a poor estimation of both the net heat of adsorption for water molecules on SiO walls and the

Table 1
Assumed post size distributions for sensors P1 and P2. (see text for details)

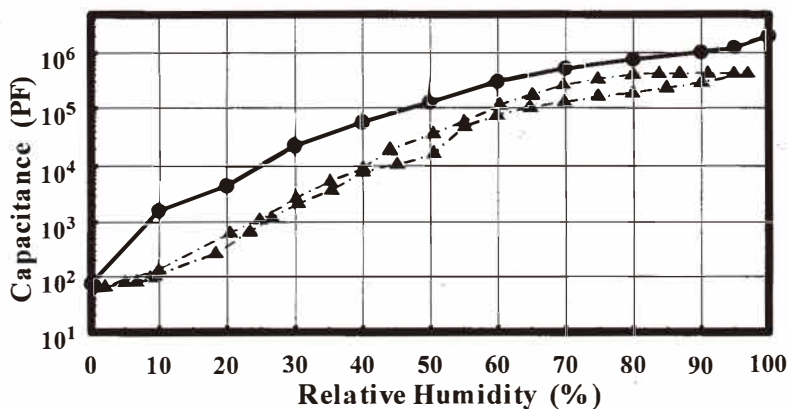| Post Size(nm)	600	300	100	50	25
Percentage(%) Sensor P1	20	30	10	15	25
Percentage(%) Sensor P2	10	20	35	20	15

Fig. 6.   Calculated C-RH curve (solid line with black dots) together with the measured C-RH curve for sensor P1.

conductivity near the water and SiO interface. These effects will be discussed separately later in this paper.

The present model is capable of explaining the unusually large change in capacitance for the following reasons: a) In this model, we treat the complex sensing system as a whole using a modification of Sillars' medium theory, in which the interactions between the SiO film, water moisture, and the applied field are automatically taken into consideration. The interactions also lead to a change of electrical conductivity near the interface between SiO and the adsorbed or condensed water molecules. b) Detailed microstructure-related parameters appear in the formulation of the model, including the post size distribution, post diameter, thickness of the adsorbed water molecule layer, and percentage of water moisture. c) Water condensation due to the capillary effect and the variation of the electrical conductivity of the condensed liquid water with the post size are also considered in the model.

3.2.2 *The stability of SiO film*

We address here the question regarding the stability of SiO films. This is important, since it concerns the performance of our RH sensors. According to ref. 13, SiO should be insoluble in both cold and hot water. It is assumed, therefore, that RH sensors made out of SiO are stable in the environment of water moisture and do not degrade even after immersion in water. This is the major motivation for selecting SiO as the RH sensing material. However, it is claimed[14] that SiO is metastable in the solid state and can be converted to SiO_2 when exposed to air, oxygen, or water vapor, particularly in the form of films deposited at oblique angles. On the other hand, SiO is found[15] to be a reasonably well characterized material when prepared in the absence of oxygen.

From our own experiments, we found that the stability of SiO film depended critically on the deposition parameters, particularly the deposition rate and base pressure. For all

SiO films deposited at base pressures less than 2.7×10^{-4} Pa and deposition rates between 20 and 40 Å/s, the composition was found to be mainly SiO based on energy dispersive X-ray (EDX) analysis within roughly two weeks of deposition. The color of these films was amber. For films deposited at higher base pressures and lower deposition rates, the color changed from an initial light amber to milky white after being in air for several weeks. EDX analysis showed that films with a milky white color are mainly SiO_2. We believe that films deposited under the latter conditions are not good for fabricating RH sensors in terms of the environmental stability and reproducibility of the sensors. This may be at least partially attributable to the easy hydration of SiO_2 when it is in contact with liquid water or in a humid environment.[16] Hydration may take place in the following way:[17] $(SiO_2)_x + 2H_2O \rightarrow (SiO_2)_{x-1} + Si(OH)_4$. This hydration process deteriorates the electrical properties of SiO_2, leading to the instability and irreproducibility of SiO_2 sensors, although the hydration rate[17] for amorphous SiO_2 is only about 100–130 ppm. Experimentally, we found that higher deposition rates produce powder-like deep brown films and are not good for fabricating RH sensors. Some sensors fabricated under suitable conditions described above still retained their amber color after remaining in ambient air for several months. Normally it is better to keep fabricated sensors inside a desiccator when the sensors are not used. Figure 7 shows two C-RH curves for sensor P1 and sensor H1 measured more than six months apart. Generally speaking, the C-RH curves shifted slightly downward after exposure to air for more than six months. We believe that this is mainly due to partial oxidation on the surfaces of the SiO posts to SiO_2, since the dielectric constant of SiO_2 (~3.8) is smaller than that (~5.8) of SiO. This type of oxidation also leads to changes in the net heat of adsorption of water molecules on the walls of the SiO posts, which may also contribute to the shift of the C-RH curves. Moreover, the SiO_2 on the surfaces of the SiO posts may also suffer from hydration as discussed above, which may affect the C-RH curves as well.
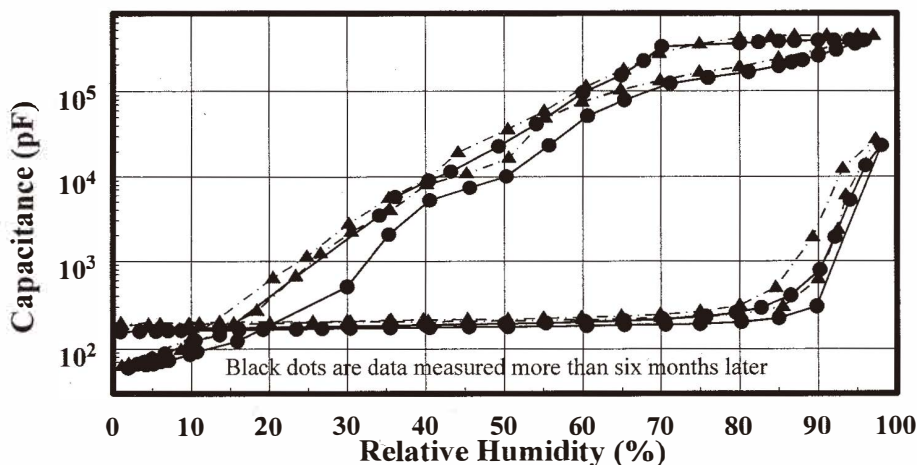

Fig. 7.   Effect of aging on sensor H1 (lower curves) and sensor P1.

3.2.3 *The net heat of adsorption*

In Section 3.2.1, we adopted a value of 2.8 kcal/mole for the net heat of adsorption of water molecules on the walls of SiO. This value is obtained from the data[12] for SiO_2, and therefore may not be accurate, although the surfaces of SiO may partially be turned into SiO_2 due to exposure to air. The uncertainty introduced here can have a large influence on the measured total capacitance. This effect is demonstrated in Fig. 8 where, as an example, the capacitance is calculated as a function of the net heat of adsorption for a RH of 50%. A change in the net heat of adsorption from –3 to 2 kcal/mole may lead to a change of capacitance over more than three orders of magnitude. However, the capacitance is relatively insensitive to a change in net heat of adsorption near the value of 2.8 kcal/mole chosen for SiO.

The value of the net heat of adsorption reflects the strength of the binding energy between the first layer of adsorbed water molecules and the walls of SiO posts. Positive and larger values reflect a stronger binding energy, while negative and smaller values reflect a weaker one. In the original derivation[18] of the BET eq. 4, it is assumed that the heat of adsorption in all layers above the first is equal to the latent heat of condensation L. This may not be true, particularly for the cases when the net heat of adsorption is negative. A more complete treatment is given in ref. 19. Nevertheless, eq. 4 can still give us some ideas about the effects of the net heat of adsorption. An important implication of Fig. 8 is that we can change the sensitivity of a sensor by modifying the interfacial properties between the porous medium and the sensed gases. Therefore, to improve the sensitivity of a porous capacitive gas sensor, one might find a means to coat the surfaces of the porous sensing medium to increase the strength of the adsorption of the gases at the surfaces. Of
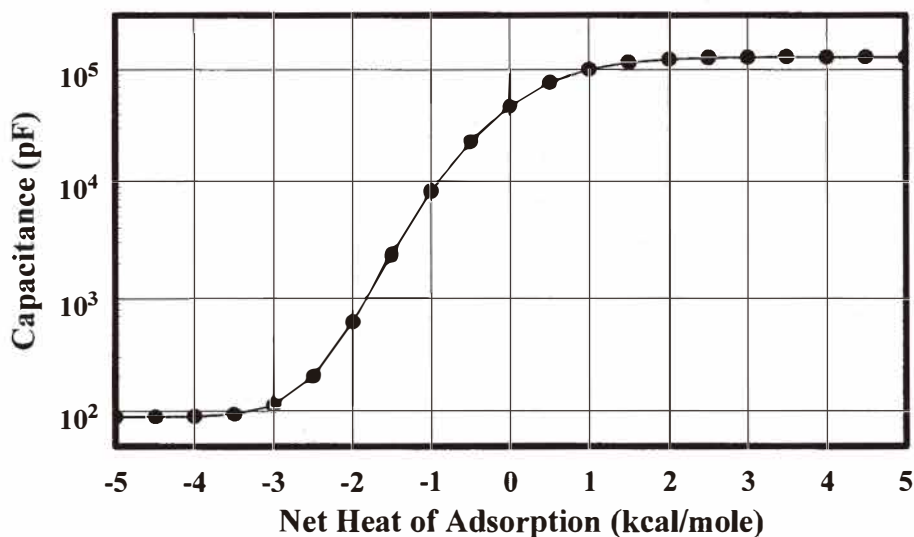

Fig. 8.   Capacitance calculated as a function of the net heat of adsorption of water molecules on the surfaces of SiO posts for Sensor P1 at a relative humidity of 50%.

course, one must also pay attention to the negative aspects of such treatment. Obviously, binding that is too strong can lead to an enhanced hysteresis loop for the C-RH curve. For our SiO RH sensors, this is not a problem since both water molecules and SiO are dipolar and the binding is therefore relatively strong. In fact, the net heat of adsorption of 2.8 kcal/mole appears to be already in the saturated region of the curve in Fig. 8. It must be noted, however, that the vertical axis of the figure is on the log scale, and therefore capacitance still increases with the increasing net heat of adsorption even above 2.8 kcal/mole.

3.2.4 *The conductivity near the interface between SiO and water molecules*

Another important factor governing the response of sensors to changes in RH is the conductivity (σ_w) near the interface between SiO and adsorbed or condensed water molecules. This effect is demonstrated in Fig. 9 where, as an example, capacitance is plotted as a function of the conductivity of adsorbed or condensed water molecules, again at a RH of 50%. Capacitance increases almost linearly with conductivity.

For liquid water, the conductivity[5] is about 8.20×10^{-5} S/m. The corresponding capacitance is only 551 pF as calculated from the model, although the model generally overestimates the total parallel capacitance as discussed earlier. This implies that some changes must occur for the adsorbed water molecules on the walls of SiO posts, leading to a remarkable increase in their conductivity. One major source responsible for this increase in the conductivity is the dissociation of water molecules on the surfaces of SiO posts. The mechanism is as follows: Once porous SiO films are exposed to air, a chemisorbed layer of water molecules forms on the surfaces of the SiO posts. Due to the high electrostatic fields in the chemisorbed layer, the subsequent physisorbed layers undergo dissociation in the following way:[20] $2H_2O \leftrightarrow H_3O^+ + OH^-$. This process of dissociation is enhanced in the
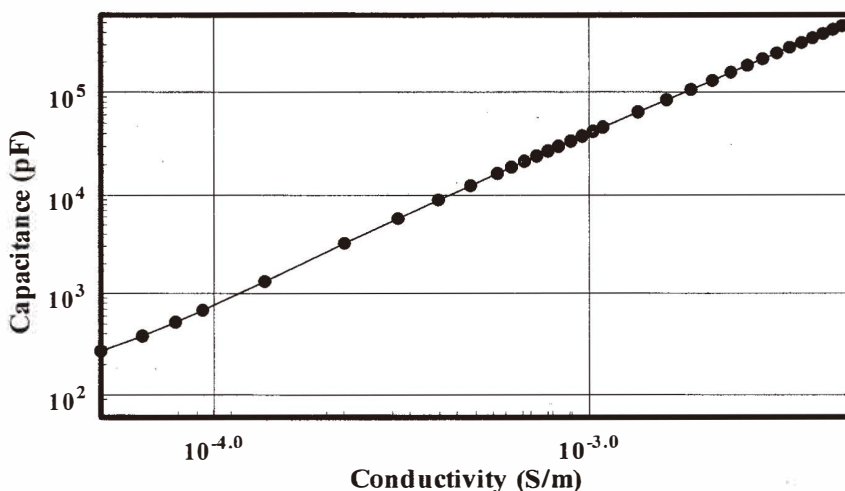

Fig. 9.   Capacitance calculated as a function of the conductivity of the adsorbed water molecules on the walls of SiO posts for sensor P1 at a relative humidity of 50%.

present case since both SiO and water molecules are dipolar in nature. Conductivity increases due to the presence of H^+, H_3O^+, and OH^- ions in the layers of adsorbed water molecules and to the Grotthuss chain reaction,[20] in which hopping of H_3O^+ occurs by releasing a proton to a nearby water molecule and transforming it into a new H_3O^+, and so forth. Although water dissociation also takes place in liquid water, the dissociation rate on the surfaces of ceramic oxides is about a factor of 10^6 larger.[21]

The conductivity of water at and near the interface between water molecules and SiO posts may vary with RH in a complicated way. When porous media are in contact with water moisture, several processes occur. With increasing RH, water molecules may adsorb on the surfaces of the pores, forming a monolayer, then multilayers, and eventually liquid water due to capillary condensation. At values of RH below $(RH)_m$, water molecules adsorbed on the walls of SiO do not form a complete electrical connection between the two electrodes. The total equivalent conductivity is almost zero due to the contribution from air, as shown in the equivalent circuit model in Fig. 5. When $RH = (RH)_m$, a complete monolayer of water molecules forms. Water molecules in this layer are doubly hydrogen-bonded to two surface hydroxyls[22] and cannot move or rotate freely. Therefore, they behave like ordered ice. For higher values of RH, multilayers of adsorbed water form. Water molecules now have more freedom to rotate due to a single hydrogen bond. On the other hand, the interactions between the water molecules and with SiO become weaker for water molecules in the higher multilayers. With these competing effects, we expect that conductivity reaches a peak at a certain distance (denoted as d_o) from the surfaces of SiO posts. Conductivity decreases when liquid water forms, particularly for larger pores. Nevertheless, the conductivity may still be larger than that of pure water due to the dissolution of some gases in air, such as CO_2 and H_2S, into the liquid water. This variation is summarized in Fig. 10. Generally speaking, the conductivity in narrow pores should be larger than that in wide pores. Guided by Fig. 10, in our model calculations these dependences are approximated and assumed as shown in Table 2 and Fig. 11 for SiO. This assignment implies that the water molecules in approximately the third layer on the surfaces of SiO posts have the highest conductivity. Clearly, different sensing materials may have different d_o.

Our analysis here implies that for optimized capacitive SiO sensors, it is better to have a microstructure with a post radius that has the equivalent Kevin radius of d_o. For a general porous capacitive RH sensor, this means that the typical radius of the pores inside the sensor must be equal to the equivalent Kevin radius of d_o to have a maximum dynamic response range at a certain porosity. Of course, in reality we have to take the influence of the microstructure on the magnitude of the hysteresis loop of the C-RH curve into account. For most applications, minimization of the hysteresis loop in the C-RH curve is much more important than having a maximum dynamic response range.

3.2.5 *The effect of applied field*

Both the amplitude and frequency of the applied field affect the measured capacitance of the sensor. However, in our model we do not consider the effect of the magnitude of the applied field based on the following consideration. Dielectric polarization mechanisms of compact thin films may generally be classified into two groups:[23] those which occur due to
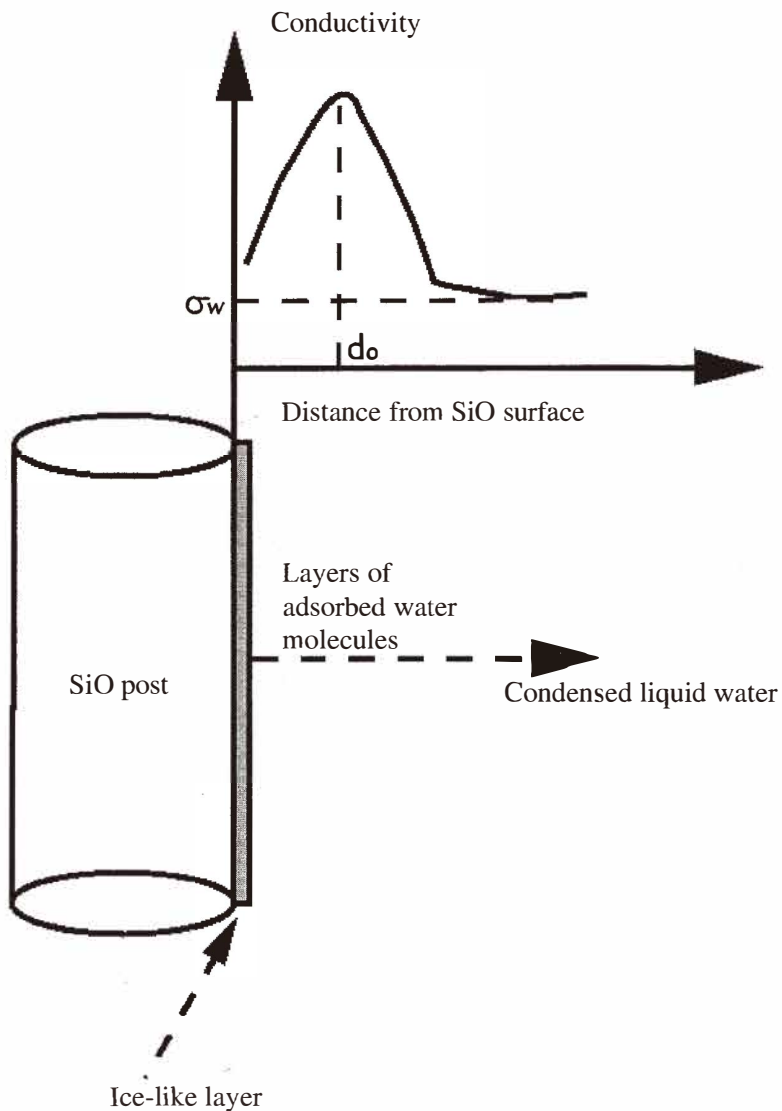
Fig. 10.   Illustration of possible behaviors of the conductivity of water molecules at and near the interface between SiO and adsorbed or condensed water molecules.

the presence of interfaces between electrodes and thin films, and those which are characteristic of the thin film material itself. For SiO films deposited at normal incidence ($\alpha = 0$), it was found[24] that the contribution to capacitance was dominated by the mechanisms of the

Table 2
Assumed variation of the conductivity of condensed water with post size.

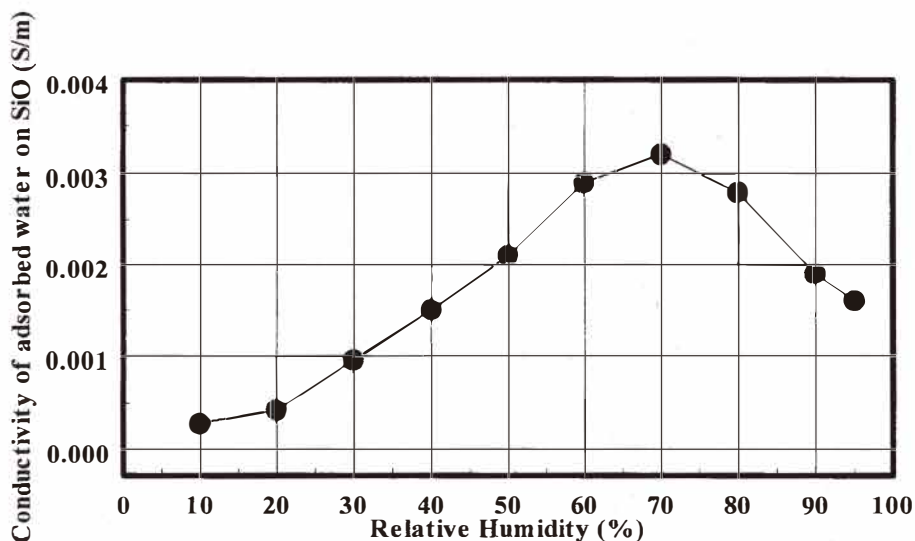| Post Size(nm)	600	300	100	50	25
σ_w (S/m)	1.7×10^{-4}	2.4×10^{-4}	7.4×10^{-4}	1.5×10^{-3}	1.7×10^{-3}

Fig. 11.   Assumed conductivity of adsorbed water molecules on the surfaces of SiO posts as a function of RH. This relationship is used for all related calculations in this paper.

first group for films with less than 2 μm thickness and probing frequencies below 100 Hz. Under this circumstance, the magnitude of the applied field affects the measured capacitance; a larger magnitude produces smaller capacitance. For thick SiO films, the contribution to capacitance is dictated by the mechanisms of the latter group, which hardly depend on the magnitude of the applied electric field as long as the magnitude does not exceed the breakdown limit of SiO, which is about 2.7 MV/cm at room temperature.[25] Since our films are much thicker than 2 μm, we may, therefore, neglect the variation of measured capacitance with the amplitude of the applied field. For films with thickness below 2 μm, the predicted C_p should be calibrated using the data in ref. 24 when the probing frequency is below 100 Hz.

The capacitance dispersion curve for sensor P1 at a RH of 50% is predicted in Fig. 12. As shown, the measured capacitance decreases dramatically as the probing frequency increases in the region between 100 and 10,000 Hz and then becomes nearly constant. This phenomenon can be understood qualitatively as follows. The polarization of a gas molecule normally has contributions from three sources: electrons, atoms, and dipoles. For
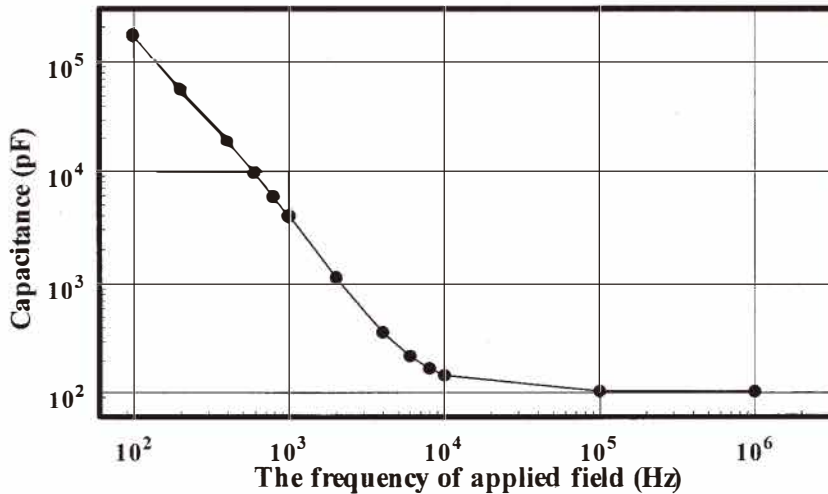
Fig. 12. Capacitance of sensor P1 is calculated as a function of the frequency of the applied electric field at a relative humidity of 50%.

water molecules, the major contribution comes from dipoles. Therefore, the measured capacitance is largest when the number of dipoles that can respond to the applied ac field is the largest. Due to various interactions existing at and near the interfaces between water molecules and SiO, which limit the rotation of water molecules as discussed in Section 3.2.4, a lower frequency allows more water molecules to respond to the alternating field, resulting therefore in a larger capacitance. When the probing frequency is larger than 10 KHz, dipoles of water molecules inside the pores can no longer respond to the change in the ac field. At this stage, the dominant contribution is from atoms and ions.

The analysis here suggests, therefore, that the lower the probe frequency, the larger the dynamic response range. It is common to apply an external DC field during a normal capacitance measurement. For our RH sensors, however, it is better not to do so when it is not necessary.

3.2.6 *The effect of microstructure*

Fabrication of porous RH sensors with controlled microstructures has been suggested in several review papers[20,22,26] as a future step towards improving the sensing characteristics of RH sensors. The recently developed GLAD technique suits this need well. First of all, vacuum deposition allows us to fabricate porous sensors without unwanted impurities and chemicals. Second, the precise control of substrate motion by computer in our GLAD set-up enables the microstructure of the sensor to be engineered on a 10 nm scale. Third, we can use virtually any dielectric substance as the sensing material. The last point is further supported by recent advances in the GLAD technique. It has been shown recently that in addition to thermal and e-beam evaporation methods,[1] GLAD films can also be

grown by sputtering[27] and laser ablation[28] methods. Therefore, with the GLAD technique, various materials may be used as the source materials to fabricate films with controllable microstructures including metals, semiconductors, dielectric materials, organic materials, and refractory materials.

The experimental results reported herein demonstrate clearly that microstructure plays an important role in determining the sensing properties of our RH sensors. Here, we show how the model accounts for varied microstructures. Taking again the post microstructure as an example, by changing the post distribution function, the radius of the post, and the average porosity, we can tune the C-RH curve as desired. Figure 13 shows two hypothetical extreme cases calculated for the same geometry as that of sensor P1. The curve with triangular points is obtained by assuming only one post size of 1 nm and a porosity of 45%, whereas the curve with square points assumes a post size of 600 nm and a porosity of 0.5%. Other parameters are the same as those for calculating the C-RH curve for sensor P1, except for the assumption of a water conductivity of 7.4×10^{-3} (S/m) for a post size of 1 nm. Conceivably any C-RH curve in between the two extreme curves in Fig. 13 can be obtained by an appropriate combination of the three microstructure-related parameters.

Generally speaking, the maximum dynamic response range is determined by the average porosity of the sensor as long as all the pores inside the sensor can be filled by water capillary condensation at saturation. More porous samples have a larger dynamic response range. This conclusion does not hold when the porosity is so large that some of the pores inside the sensor cannot be regarded as capillaries. When the porosities are the same, then sensors with smaller pore sizes will generally have larger dynamic response
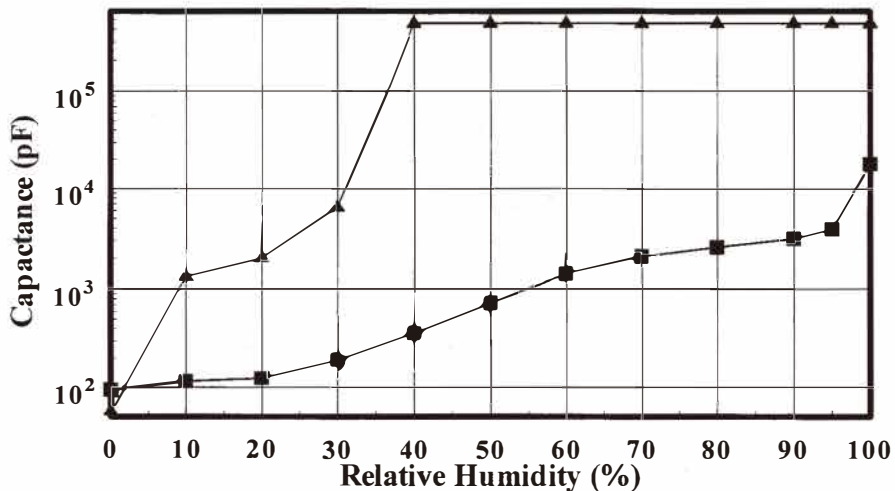

Fig. 13. C- RH curves for a sensor with a post size of 1 nm and a porosity of 45% (the upper curve) and a sensor with a post size of 600 nm and a porosity of 0.5%. In principle, any curve lying in between these two curves may be obtained by tuning the microstructure of the sensor.

ranges as long as the radii of the pores are larger than the diameter of a water molecule. Sometimes, however, sensors with appropriate pore sizes may even have the same or larger dynamic response ranges than sensors of similar or slightly larger porosities due to the effect of the conductivity of water as discussed in Section 3.2.4. Typical experimental examples in this respect are sensors H1 and H2 as shown in Section 3.1. Sensor H2 was deposited at $\alpha = 81°$, while sensor H1 at $\alpha = 83°$, and thus sensor H2 should be more compact than sensor H1. From Fig. 3(a) and Fig. 3(c) it is evident that sensor H1 contains many large pores, while the pores inside sensor H2 are smaller. Therefore, the conductivity for water at a given RH is always larger in sensor H2 than sensor H1. This is why the C-RH curve for sensor H2 lies above the corresponding curve for sensor H1. Since the tilting angle of the substrate has a more significant effect on the average porosities of the films fabricated at higher deposition angles, sensor H3 is much more porous than sensors H1 and H2 as evidenced by the SEM image shown in Fig. 3(e). This is why the C-RH curve of sensor H3 is above the curves of both sensors H1 and H2, although the pore size in sensor H3 is clearly the largest.

3.2.7 *Hysteresis*

In almost every C-RH curve discussed thus far, significant hysteresis effects appear. This is a feature highly undesirable for practical applications. We believe that the hysteresis effect observed in most porous RH sensors originates mainly from imperfections in the microstructures of the sensors. The effect of various microstructures of continuous porous media with isolated pores on the shapes of hysteresis loops has been discussed[29] by de Boer. For the convenience of discussion, we reproduce in Fig. 14 one of the imperfect microstructures illustrated for continuous porous media in ref. 29. According to eq. 1 the capillary in Fig. 14 will not be filled with liquid water on the adsorption branch of the curve if the RH is lower than the $(RH)_{r2}$ corresponding to capillary condensation taking place for r_2. The condensed water in the capillary will not be evaporated on the desorption branch of the curve until the RH is lower than the $(RH)_{r1}$ corresponding to capillary condensation taking place for r_1. Extra liquid water is trapped inside part of the capillary with larger radius during desorption, leading therefore to the observed larger capacitance for the desorption branch of the curve. However, not explained in de Boer's paper is how the air inside the part of the capillary with larger radius in Fig. 14 escapes after water condensation occurs for the capillary part with a smaller radius of r_1 on the adsorption branch at a lower $(RH)_{r1}$. In our view, the part of the capillary with larger radius must be connected to one or more capillaries of smaller radii. The trapped air inside the part of the capillary of radius r_2 during adsorption can escape only if the pressure produced by the liquid water condensed on top of the part of capillary of radius r_2 is larger than the pressure produced by the liquid water condensed inside the other capillary or one of the other capillaries connected to it.

For the present case, we deal with continuous pores with isolated sensing media, leading to a more complicated situation. Here, we explain only two typical examples of imperfections in the post microstructure of our GLAD RH sensors which can produce hysteresis loops. The ideas presented here may be generalized to other situations. Suppose that during film growth, capillaries of different radii are formed between SiO posts ideally illustrated in Fig. 15(a). The size of the capillaries is in the following order: $r_{a1} > r_{a2} > r_{a3}$
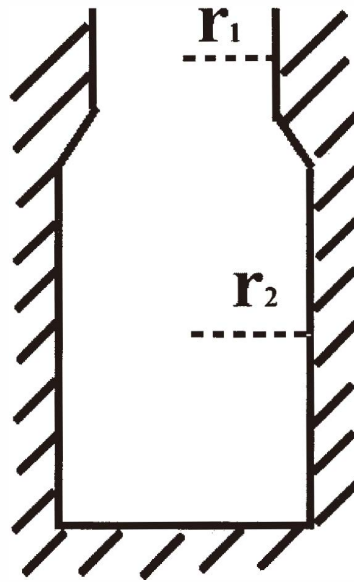
Fig. 14.   Example of the imperfect microstructures that may produce hysteresis effects in a capacitive humidity sensor using a continuous porous medium as the sensing material.

$> r_{a4} > r_{a5}$. The capillary of radius r_{a3} (called the r_{a3} capillary hereafter, with analogous abbreviations used for other capillaries) is connected to the r_{a4} and r_{a5} capillaries. During adsorption, according to eq. 1, water condensation will happens first in the r_{a5} capillary when RH reaches $(RH)_{a5}$, and then in the r_{a4} capillaries sequentially. Therefore, air is now trapped inside the capillary r_{a3} when RH reaches $(RH)_{a4}$ if the pressures at the connection between the r_{a3} capillary and each of the other capillaries connected to it are not sufficiently large to push the trapped air out through any one of the connected capillaries. With further increases in RH up to $(RH)_{a2}$, water will condense in the r_{a2} capillary. Due to the condensed water in the r_{a2} capillary, the pressure at the connection between r_{a3} and r_{a5} capillaries may be sufficiently large to push the trapped air out through the connection between r_{a3} and r_{a4}. During desorption, however, the condensed water inside the r_{a3} capillary will not empty until the RH drops below $(RH)_{a4}$. Therefore, in the RH region of $(RH)_{a2} > RH > (RH)_{a4}$, the desorption branch of the C-RH curve has a larger capacitance than the corresponding adsorption branch due to the difference in contribution between liquid water and air trapped in the r_{a3} capillary. The second example is more general and may be better explained using the idealized drawing in Fig. 15(b). Suppose that the r_{b1} and r_{b2} capillaries are formed inside the SiO posts and the size of the r_{b1} capillary is larger than that of the r_{b2} capillary. During adsorption, liquid water forms inside the r_{b2} capillary at $(RH)_{b2}$. When RH is increased, the condition for water condensation is determined by the radius (r_{m2}) of the meniscus of the liquid water at the connection between the r_{b2} and r_{b1} capillaries and the radius r_{b1}. The actual water condensation conditions depend on the ratio between the
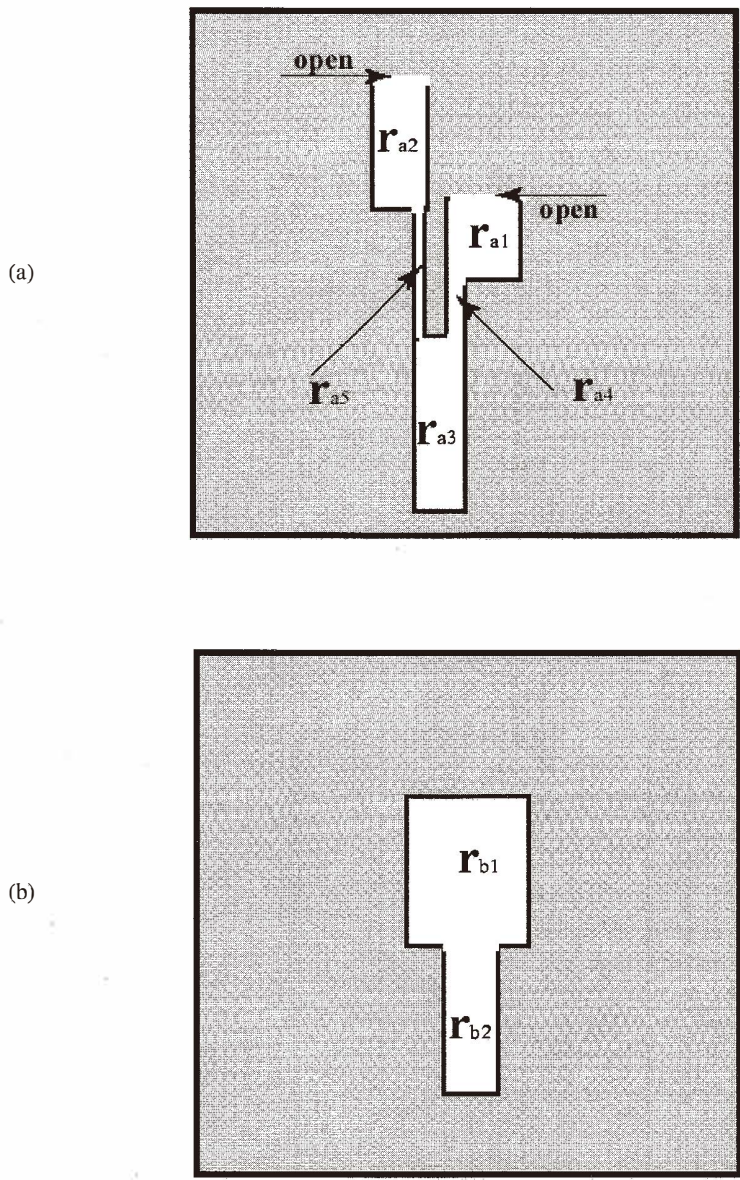
(a)

(b)

Fig. 15.   Schematic drawing of two possible imperfect microstructures in our porous SiO relative humidity sensor that may produce hysteresis effects in the C-RH curve.

surface areas of the menisci of the liquid water and the r_{b1} capillary. If this ratio is small, then liquid water only condenses when RH reaches $(RH)_{b1}$. If the ratio is larger or equal to unity, then further water condensation is determined mainly by r_{m2}. During desorption, the liquid water inside the r_{b1} capillary evaporates. The evaporating condition is determined by r_{m1} instead of r_{b1}. If r_{m1} is smaller than r_{b1}, then the capacitance in the desorption branch of the C-RH curve will be larger than the corresponding capacitance in the adsorption branch for RH in the region $(RH)_{b1} > RH > (RH)_{m1}$.

Although it is difficult to determine three-dimensional pore structures from an SEM cross-section image, examination of Fig. 16 reveals potential imperfect microstructures. The capillary indicated by arrow 1 may have trapped air in its lower part. A similar situation may occur for the capillary indicated by arrow 2. Arrow 2 indicates a common
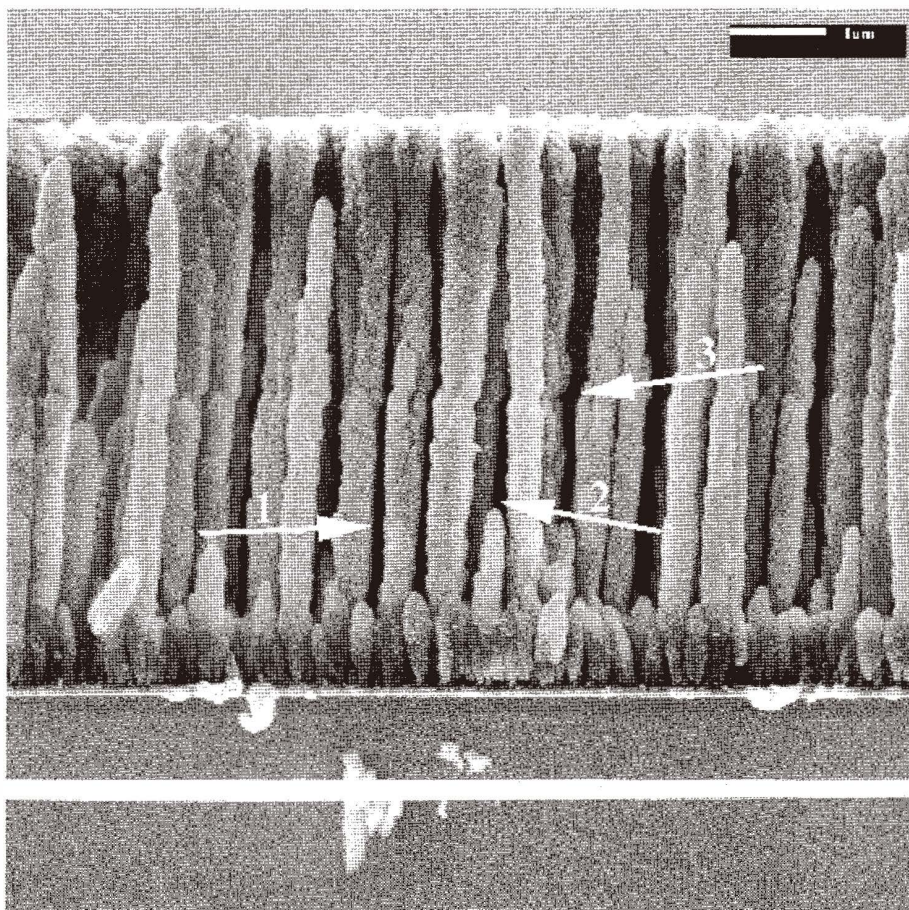

Fig. 16. Some real examples of imperfect microstructures that may produce hysteresis in sensor P1.

situation for the films grown by GLAD, wherein some posts may stop growing due to the shadowing effect from neighboring posts, creating capillaries of a relatively large size. The capillary indicated by arrow 3 may have a geometry similar to that illustrated in Fig. 15(b).

For porous media produced by other methods, particularly chemical methods such as, the anodization of Al_2O_3, the trapped chemicals inside the pores of sensors may also influence the hysteresis behavior. Chemical methods to produce porous sensors can control their microstructures only to a limited extent and may readily suffer from the "bottle neck" microstructure shown in Fig. 14.

The best way to minimize the hysteresis loop is to prepare sensors with a pore size that gradually increases from bottom to top. This allows water condensation and evaporation conditions always to be determined by the radii of the menisci of the condensed liquid water inside the pores, and there will never be any trapped air inside the sensors at any RH.

Since there are so many microstructures that may lead to hysteresis loops in C-RH curves, it is difficult to take the hysteresis effect into account in our theoretical model. In our view, this is not very important as long as we know the mechanism responsible for the hysteresis and the ways to minimize the hysteresis loops.

3.3 *Optimized results*

The major drawback to our porous SiO RH sensors is their relatively large hysteresis loops in C-RH curves. Therefore, our primary goal in optimizing our sensors is to minimize the capacitance hysteresis loops while retaining a reasonably large dynamic response range and a quick response time. An optimization of design also provides a check on the validity of the model.

To minimize the hysteresis loops, we grew SiO posts with progressively increasing radii. This was achieved by changing the deposition rate gradually from 40 Å/S near the substrate to 20 Å/S at the top of the uncapped films while maintaining a constant substrate rotation speed. In this manner, the substrate rotation speed relative to the deposition rate was increased by a factor of two from the beginning to the end of the film deposition. Experimentally, it was found that the large deposition rate and relatively slow spinning rate of the substrate prevent a compact layer, such as the bottom part in Fig. 16, from forming. The deposition rate is decreased gradually as the film thickness increases, which allows the typical dimensions of the capillaries inside the SiO posts to grow gradually larger from the bottom to the top. In order to approach a close-packed situation to minimize errors during calculations employing our theoretical model shown in Section 3.2, the films were grown at the deposition angle $\alpha = 83°$.

One example of a cross-section of the optimized sensors is shown in Fig. 17(a). The microstructure of the optimized sensor is not very well illustrated in this figure due to the deleterious effects of cleaving the capping layer during SEM specimen preparation. The corresponding SEM image before depositing the capping layer is shown in Fig.17(b). From the images, we believe that we have at least partially fulfilled our goal for the microstructure. The film appears reasonably compact for deposition at such an angle. However, this may be due in part to the uncertainty (~2°) in determining the deposition angle. The C-RH for this sensor is shown in Fig. 18. As one may see, the hysteresis loop is almost eliminated and the dynamic response range is still over five orders of magnitude.
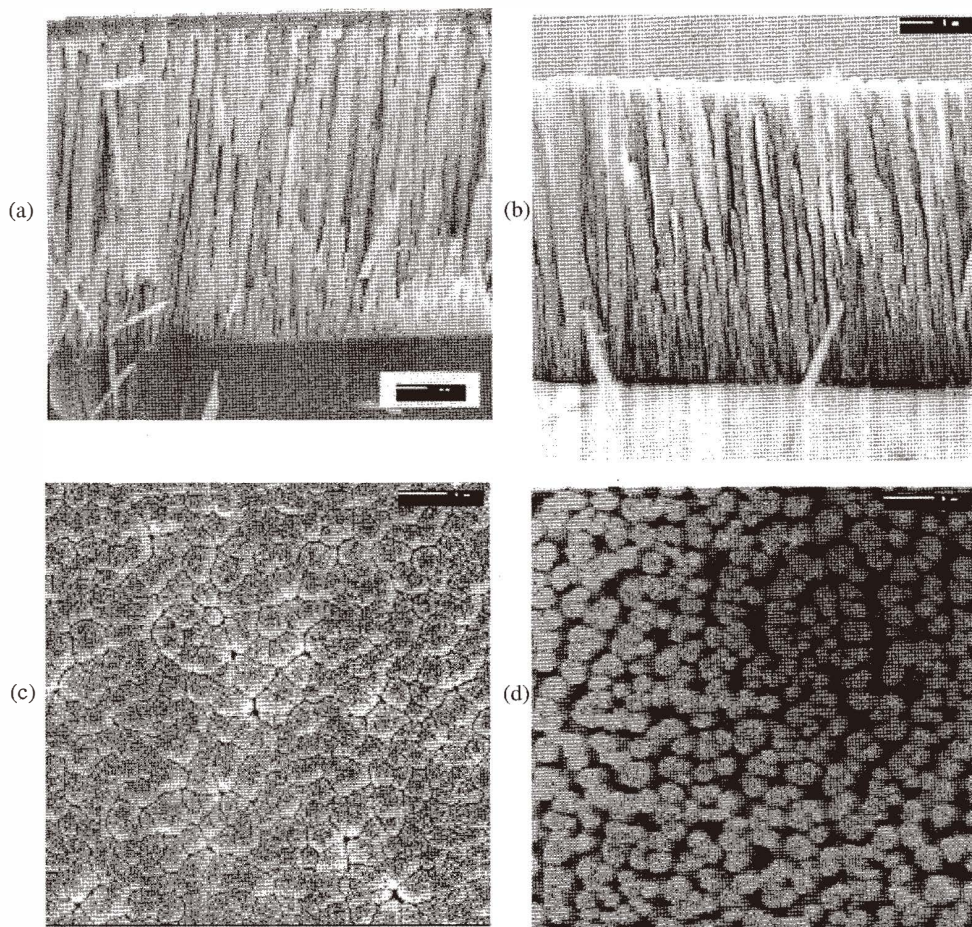
Fig. 17. SEM cross-section images of sensor P2 a) after capping and b) before capping. SEM top-view images of sensor P2 c) after capping and d) before capping.

The response time of our porous GLAD sensors is controlled mainly by the surface porosity of the sensors.[3] The top view of this optimized sensor is shown in Figs. 17(c) and 17(d) for the sensor before and after capping, respectively. The average porosity can be estimated from Figs. 17(d) to be 12%, which is near the close-packed density. From Fig. 17(c), we see that the pores or orifices are homogenously distributed on the surface with most of the sizes being larger than the diameter of water molecules (~3.87 Å). The response time for a step change in RH from 15% to 80% for this sensor is a few seconds slower than that for sensor P1, which is still better than most of the available RH sensors on the market. The response time can be improved further if we make the sensor smaller and thinner.
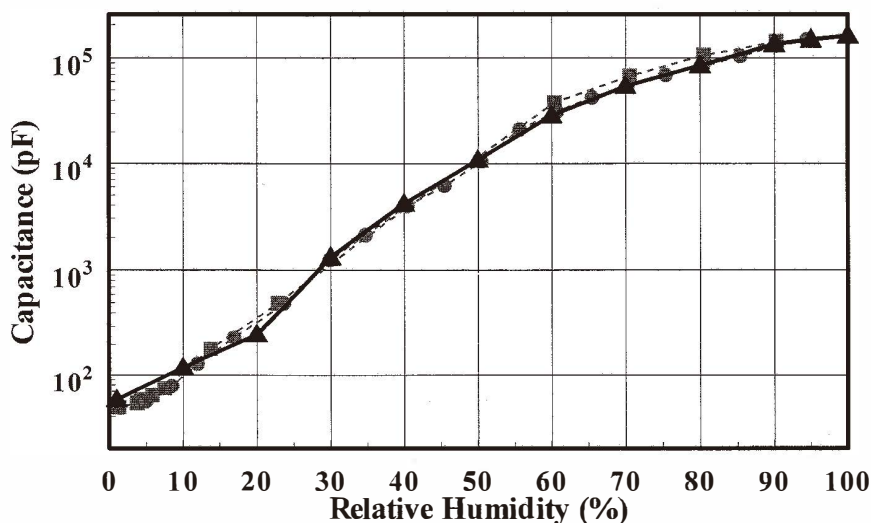
Fig. 18.   Measured and calculated (solid line with black triangles) C-RH curves for sensor P2.   The data with dots are for increasing relative humidity, whereas squares are for decreasing relative humidity.

The theoretical C-RH curve is also shown in Fig. 18 as the solid curve with triangular points.   The fit is of course better than that for sensor P1, since the density of the optimized sensor (sensor P2) is closer to the close-packed situation.   The assumed pore size distribution function for sensor P2 based on the SEM images of Figs.17(a) and 17(b) is given in the last row of Table 1, and the rest of the parameters used for calculations are the same as those used for sensor P1.

4.   Conclusions

Details of the processes for the developing of a novel capacitive relative humidity (RH) sensor based on porous SiO films fabricated by employing the advanced GLancing Angle Deposition (GLAD) technique are described in this paper.   The GLAD technique enabled the microstructures of the porous sensors to be controlled in three dimensions on a 10 nm scale and also the tuning of the porosity as desired.   A theoretical model was constructed to explain the observed sensing characteristics of our sensors, particularly the unusually large dynamic response range.   It was found that the sensor properties are mainly determined by the detailed microstructures of the sensors, the properties of the surfaces of SiO posts, and the properties at or near the interfaces between SiO posts and the adsorbed water molecules or condensed liquid water in the pores of the sensors.   Effects from the net heat of adsorption of water molecules and the applied electric field on the sensing characteristics

were also considered and discussed. This theoretical model was found to explain the major experimental features self-consistently.

Although the model was developed for explaining our sensors, it is reasonably general and can be used to explain the sensing mechanisms for other porous capacitive RH sensors with slight modifications. The model provides guidance for fabricating optimal capacitive RH sensors using porous media. Using this guidance, we have successfully optimized the performance of our porous SiO RH sensors, particularly in relation to reducing hysteresis and maintaining a wide dynamic response. The maximum difference in capacitance between desorption and adsorption in the capacitive-RH curve of the optimized sensors is typically below 15%. The dynamic response range is over five orders of magnitude with a response time for a step change of RH from 15% to 80% in a few seconds.

Acknowledgement

References

1   K. Robbie and M. J. Brett: J. Vac. Sci. Technol. A **15** (1997) 1460, United States patent 5866204.
2   A. T. Wu, M. J. Brett, A. Huizinga and M. Seto: Proceedings of the 1999 IEEE Canadian Conference on Electrical and Computer Engineering (1999) p. 1662.
3   A. T. Wu, M. Seto and M. J. Brett: Sensors and Materials **11** (1999) 493.
4   R. K. Nahar, V. K. Khanna and W. S. Khokle: J. Phys. D: Appl. Phys. **17** (1984) 2087.
5   Y. Shimizu, H. Arai and T. Seiyama: Sensors and Actuators **7** (1985) 11.
6   G. Q. Li, P. T. Lai, M. Q. Huang, S. H. Zeng, B. Li, and Y. C. Cheng: J. App. Phys. **87** (2000) 8716.
7   V. K. Khanna and R. K. Nahar: Sensors and Actuators **5** (1984) 187.
8   R. W. Sillars: J. Inst. Elec. Eng. **8** (1937) 378.
9   K. Robbie, J. C. Sit and M. J. Brett: J. Vac. Sci. Technol. B **16** (1998) 1155.
10   D. H. Everett, The structure and properties of porous materials, D. H. Everett and F. S. Stone (Eds.), Butterworths Scientific Publications, London, (1958) p. 96.
11   S. Brunauer, L. E. Copeland and D. L. Kantro: The solid-gas interface, Vol.1, E. A. Flood (Ed.), Marcel Dekker Inc., New York, (1967) p. 96.
12   N. K. Nair and J. M. Thorp: Trans. Faraday Soc. **61** (1965) p. 962.
13   Handbook of Chemistry and Physics 56th edition, (R.C. Weast (Ed.) Chemical Rubber Co., Ohio (1975/1976) p. B-137.
14   Handbook of Thin Film Technology, eds. Maissel and Glang (McGraw-Hill, New York, 1970) p.19-9 .
15   Handbook of Optical Constants of Solids (Academic Press Inc., 1985) p. 765.
16   M. J. Madou and S. R. Morrison: Chemical sensing with solid state devices (Academic Press, Inc., San Diego, 1989) p. 150.
17   R. K. Iler: The chemistry of silica (John Wiley & Sons, Inc. USA & Canada, 1979) p. 4.
18   S. Brunauer, P. H. Emmett and E. Teller: J. Amer. Chem. Soc. **60** (1938) 309.

19   S. Brunauer, L. S. Deming, W. E. Deming and E. Teller: J. Amer. Chem. Soc. **62** (1940) 1723.

20   B. M. Kulwicki: J. Am. Ceram. Soc. **74** (1991) 697.

21   W. J. Fleming: Proceedings of the international automotive meeting (Detroit, USA, 1981) p. 51.

22   N. Yamazoe and Y. Shimizu: Sensors and Actuators **10** (1986) 379.

23   C. H. S. Dupuy and A. Cachard: Physics of nonmetallic thin films (Plenum Press, New York, 1976) p. 225.

24   J. Roger and C. H. S. Dupuy: J. Appl. Phys. **46** (1975) 3102.

25   J. J. O'Dwyer: The theory of electrical conduction and breakdown in solid dielectrics (Claredon Press, Oxford, 1973) p. 194.

26   J. G. Fagan and V. R. W. Amarakoon: Am. Ceram. Soc. Bull. **72** (1993) 119.

27   J. C. Sit, D. Vick, K. Robbie and M. J. Brett: J. Mater. Res. **14** (1999) 1197.

28   D. Vick, Y. Y. Tsui, M. J. Brett and R. Fedosejevs: Thin Solid Films **350** (1999) 49.

29   J. H. de Boer: The structure and properties of porous materials, eds. D. H. Everett and F. S. Stone (Butterworths Scientific Publications, London, 1958) p. 68.